Biophysical Journal
Article

Biophysical Society

Airway Bistability Is Modulated by Smooth Muscle Dynamics and Length-Tension Characteristics

Graham M. Donovan[1,*]
[1]Department of Mathematics, University of Auckland, Auckland, New Zealand

ABSTRACT Airway closure has important implications for lung disease, especially asthma; in particular, the prospect of bistability between open and closed (or effectively closed) airway states has been thought to play a prominent role in airway closure associated with the formation of clustered ventilation defects in asthma. However, many existing analyses of closure consider only static airway equilibria; here we construct, to our knowledge, a new model wherein airway narrowing and closure dynamics are modulated by coupling the airway to cross-bridge models of airway smooth muscle dynamics and force generation. Using this model, we show that important qualitative features of airway pressure-radius hysteresis loops are highly dependent on both airway smooth muscle dynamics, and the length-tension relationship. Furthermore, we show that two recent experimental results from intact bronchial segments are both expressions of the same phenomenon: that a monotonically increasing length-tension relationship, with sharply higher tension at longer lengths, is needed to drive the observed changes in low-compliance regions of the baseline pressure-radius curve. We also explore the potential implications of this finding for airway closure in coupled airway models.

INTRODUCTION

Bistability in airways between open and closed states has long been studied for its potential to help understand airway closure in asthma. There are several distinct, yet related, ideas: static bistability, either in an isolated airway (1) or in a terminal airway unit with coupled parenchymal tethering (2); dynamic coupling of the airway with airway smooth muscle (3–5); and mechanisms by which spatial organization of airway closure or near closure may lead to clustered ventilation defects (6,7). All are interrelated, but as of yet there is no integrated synthesis of all three mechanisms.

Here we are motivated to consider the ways in which airway smooth muscle (ASM) dynamics may modulate this bistability. This is driven by two recent studies on intact bronchial segments, which together challenge our expectations of how ASM dynamics might modulate the transitions between open and closed airway states (8,9). This could have profound consequences for our understanding of airway closure in disease. In the absence of activated ASM, the quasi-static airway pressure-radius curve is known to have a characteristic shape, sigmoidal in small airways with a highly compliant region, and progressively flattening for larger airways (e.g., Harvey et al. (8), Lambert et al. (10), and LaPrad et al. (11); see Fig. 1 *a* for representative curves). Also of interest is the hysteresis shown as the airway is inflated and deflated, which originates both with viscous equilibration mechanisms, but also because of transitions between bistable open and closed airway states. A key question is how this hysteresis relationship is altered by ASM activation. One might suppose that several results are possible: for example, either a simple shift of the passive curves corresponding to higher force; or perhaps a widening of the hysteresis loop in the highly compliant region, where changes are relatively easier to affect, but with little change in the less compliant regions of the pressure-radius curve.

Recent evidence casts doubt on these simple interpretations. In particular, the deflation pressure-radius curves measured by Harvey et al. (8) in intact bronchial segments display a markedly different character, showing instead sharp reductions in radius with ASM activation in the less compliant plateau regions, and less so in the highly compliant region. This may imply an effective ASM tension curve that rises sharply at longer ASM lengths. More recently, Gazzola et al. (9) have used a different protocol, also in intact segments, to measure the ASM tension and found, qualitatively, exactly these sharp rises in tension

Submitted May 27, 2016, and accepted for publication October 5, 2016.
*Correspondence: g.donovan@auckland.ac.nz
Editor: Jeffrey Fredberg.
http://dx.doi.org/10.1016/j.bpj.2016.10.007

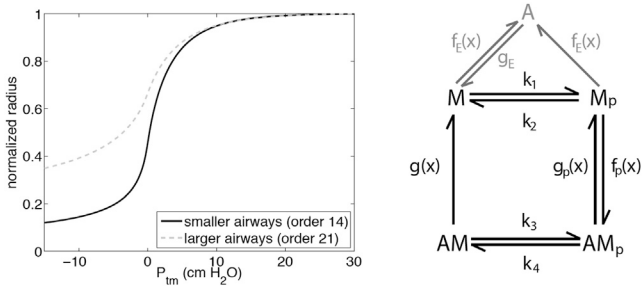

FIGURE 1 Model concept illustrations. (*Left*) Typical airway static pressure-radius curves (10,20). The solid curve is typical of smaller airways, and the dashed shaded curve is typical of larger airways. Here we have used orders 14 and 21, respectively, using the Horsfield classification scheme (27). (*Right*) Schematic illustration of the ASM cross-bridge model structure. The states are as follows: M, myosin unbound, unphosphorylated; M_p, myosin unbound, phosphorylated; AM_p, bound, phosphorylated; AM, bound, unphosphorylated; and A, isolated actin; binding site unavailable. The solid region is the core cross-bridge model, while the shaded addition is the filament overlap modification introduced by Donovan (21). Setting $g_E = f_E \equiv 0$ eliminates the shaded portion and restores the standard cross-bridge model ($A \equiv 0$).

at longer lengths. Taken together, this suggests the need for a new model that accounts for these observations, and allows us to consider both their origins and potential consequences.

In this study, we construct, to our knowledge, a new model of airway narrowing coupled with ASM constriction, wherein airway opening and closing transitions are modulated by coupling to a cross-bridge model of ASM. We first show that existing models of cross-bridge ASM length-tension behavior, when coupled to the airway, are consistent with the naive interpretation of hysteresis opening predominately in the highly compliant region of the pressure-radius curve, but at odds with the findings of Harvey et al. (8). To investigate this discrepancy, we modify the model to compute the implied ASM length-tension curves needed to generate the experimental deflation curves, and find the sharp rise in tension at longer lengths described by Gazzola et al. (9). Furthermore, we show that one possible explanation for such implied ASM length-tension curves is that the ASM is operating in situ at lengths considerably shorter than the optimal ASM length, and hence confined to only the lower half of the ascending branch of the traditional bell-shaped length-tension curve (12).

These implied length-tension curves suggest that modulation of the transitions between open and closed states, via ASM dynamics, plays a significant role; and that hysteresis loops are likely to open across a much broader part of the (relaxed) pressure-radius curve, not merely confined to the highly compliant portion. This suggests, on the whole, that individual airways may be more susceptible to narrowing than to closure; if so, this could have important implications for models that rely on the open-closed transitions (or at least functional closure) to drive clustered ventilation defects (6,7).

MATERIALS AND METHODS

Model

Motivation

There are arguably two key analyses of static airway bistability: those of Anafi and Wilson (2,3), and Affonce and Lutchen (1). Although the physiological motivations differ in important ways, in both cases the crux of the analysis is a balance between the constricting force of ASM, and the restoring forces of the airway wall (and parenchymal tethering). The underlying mathematical structure of both studies is surprisingly similar: pressure associated with the ASM scales as $\sim 1 + 1/r$, and the balancing pressures are represented by a high order polynomial (cubic or higher in r). If the parameters are such that these curves have multiple intersections, then multiple (static) equilibria are possible. Because much of the physiological range of parameter space does allow multiple equilibria, this bistability has often been used to explain the occurrence of ventilation heterogeneity and clustered ventilation defects (6,7). However, these largely static representations contain incomplete information about how these states may be modulated by ASM dynamics. Other studies have considered coupled dynamics in the context of narrowing, rather than closure (notably the work of Hiorns et al. (4,5)), or with highly simplified ASM representations (3).

To consider how these dynamics modulate closure and reopening, we extend a model of this type by coupling to it a cross-bridge model of ASM dynamics. This section is organized as follows: first, we present a brief review of existing ASM cross-bridge models; second, we present the airway wall model; and finally, we discuss the coupling between the two, which gives rise to the combined model used in this study.

ASM cross-bridge models

The history of ASM cross-bridge models originates with Huxley's sliding filament theory for striated muscle (13), with key extensions by Hai and Murphy (14) and reaching its modern form with the spatially extended ASM model of Mijailovich et al. (15) (and further extensions (16–18)). Because the ASM length-tension relationship is key to this analysis, we also consider two variations of the cross-bridge model of Mijailovich et al. (15), which offer extensions to account for length-tension measurements in ASM strips (e.g., Wang et al. (19)): principally an empirical length-tension transfer function (e.g., Politi et al. (20)) and an extension to the standard cross-bridge model that uses filament length distributions and binding site availability to generate the characteristic length-tension shape (21).

Because of their similarities, all three models can be expressed in a common framework, illustrated schematically in Fig. 1 *b*. The underlying idea in all cases is the relative sliding of actin and myosin filaments, and their phosphorylation and binding to one another. Thus the populations are as follows: M, myosin unbound, unphosphorylated; M_p, myosin unbound, phosphorylated; AM_p, bound, phosphorylated; AM, bound, unphosphorylated; A, isolated actin, binding site unavailable. (For more background details see, for example, Keener and Sneyd (22).) The governing equations are then given by the following set of hyperbolic partial differential equations (PDEs):

$$\frac{\partial M}{\partial t} - v(t)\frac{\partial M}{\partial x} = k_2 M_p + g(x)AM - (k_1 + f_E(x))M + g_E A, \tag{1}$$

$$\frac{\partial M_p}{\partial t} - v(t)\frac{\partial M_p}{\partial x} = k_1 M + g_p(x)AM_p - \big(f_E(x) + k_2 + f_p(x)\big)M_p, \tag{2}$$

$$\frac{\partial AM}{\partial t} - v(t)\frac{\partial AM}{\partial x} = k_4 AM_p - (k_3 + g(x))AM, \tag{3}$$

$$\frac{\partial AM_p}{\partial t} - v(t)\frac{\partial AM_p}{\partial x} = k_3 AM + f_p(x)M_p - \big(k_4 + g_p(x)\big)AM_p, \tag{4}$$

$$\frac{\partial A}{\partial t} - v(t)\frac{\partial A}{\partial x} = f_E(x)\big(M + M_p\big) - g_E A, \tag{5}$$

subject to the conservation equation

$$M(x,t) + M_p(x,t) + AM(x,t) + AM_p(x,t) + A(x,t) \;=\; 1.$$

Here the constants k_{1-4} and g_E, along with the functions $f_p(x)$, $g(x)$, $g_p(x)$, $f_E(x)$, and $g_E(x)$ define the transitions between states (for more detail, see Donovan (21) and Keener and Sneyd (22)). Note that setting $g_E = f_E \equiv 0$ restores the standard cross-bridge model ($A(x,t) \equiv 0$).

The relative filament velocity v is related to the muscle length L by

$$-\gamma\frac{dL(t)}{dt} \;=\; v(t),$$

where the proportionality constant scales as

$$\gamma \;=\; \gamma_0/(2\pi r_0) \tag{6}$$

to account for the arrangement of contractile units, where r_0 is the maximal ASM radius (20).

Then the ASM force is given by

$$\kappa \;=\; \widehat{\kappa}\, F_L(r(t)) \int_0^\infty x\big[AM(x,t) + AM_p(x,t)\big]\, dx, \tag{7}$$

using the standard assumption that both bound states exert force equally, and in proportion to their first moments—but with two modifications. First, we have explicitly incorporated the empirical force-length relationship via the transfer function $F_L(r)$; and second, we have truncated the moment integral to $x \geq 0$ to reflect the inability of ASM to exert a negative force opposing shortening. All three ASM models are represented by this general framework, with their different binding rate functions and parameters; details are given in Table 1.

Airway wall model

We construct the airway wall model for coupling to the ASM cross-bridge model as follows. We begin with the static airway wall model of Lambert et al. (10), which is supported by more recent experimental evidence (8,11); qualitatively similar empirical models (23) and solid mechanics models (4) also exist. Rewriting the static model of Lambert et al. (10) in terms of airway radius, this gives us

$$R(P) \;=\; \begin{cases} \sqrt{R_i^2\left(1 - P/P_1\right)^{-n_1}}, & P \leq 0 \\ \sqrt{r_{\text{imax}}^2 - \left(r_{\text{imax}}^2 - R_i^2\right)\left(1 - P/P_2\right)^{-n_2}}, & P > 0, \end{cases} \tag{8}$$

where P is the transmural pressure and the parameters depend upon airway size (20). Assuming that this static relationship holds at equilibrium, we then employ a general method of approaching these equilibria. We use the notation r for the (time-dependent) airway radius, and R for the equilibrium radius, and impose dynamics as

$$\frac{dr}{dt} \;=\; \rho[R(P) - r], \tag{9}$$

which for $\rho > 0$ then has stable fixed points at the open and closed states from the static analysis (as in Dowie et al. (24)). Coupling to the ASM

TABLE 1 ASM Model Details

	Standard Cross Bridge (15)	Empirical L-T (20)	Filament Overlap (21)
$F_L(r)$	1	$\sin^3\left(\frac{\pi}{2}\frac{r}{R_{\text{ref}}}\right)$	1
γ_0	25	25	44
$f_E(x)$	0	0	$\not\equiv 0$; see Donovan (21)
g_E	0	0	3×10^{-5} (1/s)
k_1	0.06 (1/s)	0.06 (1/s)	0.06 (1/s)
k_2	0.1 (1/s)	0.1 (1/s)	0.1 (1/s)
k_3	0.06 (1/s)	0.06 (1/s)	0.06 (1/s)
k_4	0.1 (1/s)	0.1 (1/s)	0.1 (1/s)
$f_p(x)$	$= \begin{cases} 0, x<0 \\ f_{p1}x/h, x\in[0,h] \\ 0, x>h \end{cases}$	$= \begin{cases} 0, x<0 \\ f_{p1}x/h, x\in[0,h] \\ 0, x>h \end{cases}$	$= \begin{cases} 0, x<0 \\ f_{p1}x/h, x\in[0,h] \\ 0, x>h \end{cases}$
f_{p1}	0.88 (1/s)	0.88 (1/s)	0.88 (1/s)
$g_p(x)$	$= \begin{cases} 4(f_{p1}+g_{p1}), x<0 \\ g_{p1}x/h, x\in[0,h] \\ 4g_{p1}x/h, x>h \end{cases}$	$= \begin{cases} 4(f_{p1}+g_{p1}), x<0 \\ g_{p1}x/h, x\in[0,h] \\ 4g_{p1}x/h, x>h \end{cases}$	$= \begin{cases} 3(f_{p1}+g_{p1}), x<0 \\ g_{p1}x/h, x\in[0,h] \\ 4g_{p1}x/h, x>h \end{cases}$
g_{p1}	0.22 (1/s)	0.22 (1/s)	0.22 (1/s)
$g(x)$	$= \begin{cases} 20g_1, x<0 \\ g_1x/h, x\in[0,h] \\ 4g_1x/h, x>h \end{cases}$	$= \begin{cases} 20g_1, x<0 \\ g_1x/h, x\in[0,h] \\ 4g_1x/h, x>h \end{cases}$	$= \begin{cases} 20g_1, x<0 \\ g_1x/h, x\in[0,h] \\ g_1, x>h \end{cases}$
g_1	0.01 (1/s)	0.01 (1/s)	0.03 (1/s)
h	1	1	1

This table gives rate functions and constants for the ASM models. Airway wall model parameters are drawn from Politi et al. (20) for order-dependent static parameters (R_i, P_1, P_2, n_1, n_2, r_{imax}). Throughout, we use $\rho = 1$ (1/s) and $r_0 = R(25\ \text{cmH}_2\text{O})$. We also use Horsfield order to classify airway size (27); briefly, the smallest airways are of the smallest order, with the largest airways in humans being ~25.

cross-bridge model comes via the contribution of ASM tension to constricting the airway, as

$$P = P_0 - \frac{\kappa}{r}, \tag{10}$$

with the $1/r$ dependence arising from the thin-walled Laplace law approximation (1,25) and where P_0 is the equivalent passive transmural pressure. For purposes of comparison with experiments on excised airways, we have opted for direct inclusion of the transmural pressure, rather than explicit inclusion of parenchymal tethering. However, it would be straightforward to incorporate a parenchymal tethering treatment based on Lai-Fook (26).

Model coupling and numerical solution

The ASM and airway wall models are interconnected by the relationship between ASM length and airway radius, and the contribution of ASM tension to the constricting pressure. For the former, we have $r = 2\pi L$ and so $v = -\gamma(dL/dt) = -2\pi\gamma(dr/dt)$; for the latter, we have Eqs. 10 and 7 substituted into Eq. 9.

The model is solved numerically by using the method of characteristics to reduce the cross-bridge PDEs (Eqs. 1–5) to a system of ordinary differential equations (ODEs) without introducing artificial numerical dispersion, a standard technique for models of this type. Discretizing the cross-bridge displacement variable x using N_x equally spaced points, this yields $5N_x$ ODEs for the ASM model alone, and when augmented with Eq. 9 we have $5N_x + 1$ ODEs to solve. These are relatively stiff and can display loss of order with Runge-Kutta methods, and so must be carefully convergence tested. Explicitly, changing variables along the characteristics

$$\begin{aligned}\xi &= x - \int_0^t v(\tau)d\tau = x + 2\pi\gamma[r(t) - r(0)] \\ &= x + \frac{\gamma_0}{r_0}[r(t) - r(0)]\end{aligned} \tag{11}$$

transforms the PDEs (Eqs. 1–5) into ODEs, now with ξ as a parameter. These ODEs are then discretized in ξ, yielding ODEs, which now depend not on muscle length or velocity ($v(t)$ or $L(t)$) but instead airway radius ($r(t)$). These equations are then augmented by

$$\frac{dr}{dt} = \rho[R(P_0 - \kappa/r) - r], \tag{12}$$

(arising from substituting Eq.10 into 9), where κ is given by Eq. 7 (and depends on the full cross-bridge model state), completing the governing set of ODEs. This system is size $5N_x + 1$ for the filament overlap model, but for the standard cross-bridge models where $A(x,t) \equiv 0$, Eq. 5 is discarded and the system is size $4N_x + 1$. The system size can be reduced further by exploiting the algebraic constraint and/or rate equivalence ($k_1 = k_3$ and $k_2 = k_4$).

RESULTS AND DISCUSSION

Airway pressure-radius hysteresis

We first compute families of quasi-static pressure-radius (P-R) hysteresis curves using our three ASM model variants to account for differing length-tension treatments. Mimicking the protocol of Harvey et al. (8), we cycle between 30 cmH_2O, and -15 cmH_2O with an 80 s period with a constant rate of pressure change (only changing sign for inflation/deflation). Examples of the resulting P-R curves are given in Fig. 2: the left-hand column shows variations in the degree of ASM activation (with airway size fixed), while the right-hand column gives changes in airway size (with ASM activation fixed); the rows are, from top to bottom, the standard cross-bridge model (15); the standard cross-bridge model with an empirical length-tension relationship; and the filament overlap model. Although there are differences, certain qualitative commonalities stand out. In particular, it is notable that 1) the hysteresis loops open predominantly in the highly compliant part of the baseline P-R curve; 2) ASM activation has little or no effect on the low compliance plateau above 10 cmH_2O; and 3) larger (less compliant) airways systematically exhibit less hysteresis.

These observations are important, in part, for their stark contrast with the recent data of Harvey et al. (8), which show instead a significant constriction response in the low-compliance plateau (and less so in the higher-compliance transition region). This begs the question: if our existing characterization of ASM length-tension behavior is inadequate to explain intact quasi-static pressure-radius (QSPR) curves, then what sort of ASM length-tension behavior is needed?

Implied ASM length-tension relationship

To answer this question, we use the notion of our empirical length-tension transfer function ($F_L(r)$; see Eq. 7), but now with a more general form. That is, we use a parameterized form with four evenly spaced anchor points, and a piecewise cubic interpolating polynomial between these. The model simulated deflation PR curves are then fitted to the deflation data of Harvey et al. (8) using the tension values at the anchor points; this is done for both smaller and larger airways, with airway sizes selected to match the passive QSPR curves (order 14 for smaller airways, and 21 for larger). The implied L-T curves, and resulting deflation PR curves, are given in Fig. 3.

Here ASM activation alters airway behavior in qualitatively different ways from the model results previously shown in Fig. 2; most notable are the differential effects of constriction, with large changes in the relatively flat part of the QSPR curve above 10 cmH_2O, and much smaller changes through the high compliance region. This is true for both larger airways, seen in Fig. 3 *a*, and for smaller airways in Fig. 3 *b*. The tension required to create changes of this character is illustrated in Fig. 3, *c* and *d*. Fig. 3 *c* shows the implied ASM tension transfer function, which is a piecewise cubic interpolant based around four evenly spaced nodes (with separate curves for both larger and smaller airways). However, the large and small airway curves are treated separately, as in Harvey et al. (8), where they have a similar shape up to a multiplicative scaling factor; see Fig. 4 *a*. This suggests that the difference between the large

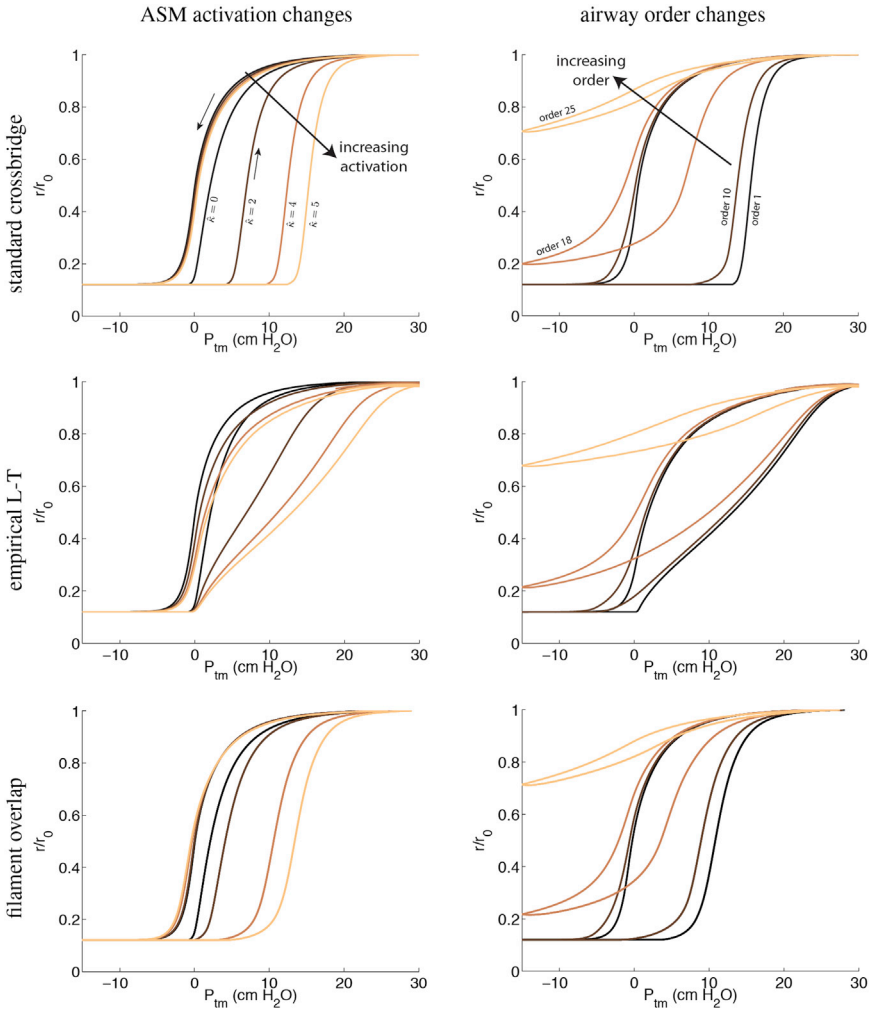

FIGURE 2 Pressure-radius hysteresis curves, illustrating changes in ASM model, ASM activation, and airway order. The left-hand column shows changes in ASM activation (with airway order fixed); the right-hand column shows changes in airway order, but with ASM activation fixed (*dark curves* correspond to smaller airways, *lighter curves* to larger airways; annotations are provided in the first row only, with the same color scheme as used in subsequent figures). Each row corresponds to a different ASM model, as labeled. Changes in parameter values are indicated in the annotations in the first row, with the same values used in subsequent rows. In the left-hand column, the airway order is 5; in the right-hand column, $\widehat{\kappa} = 5$. To see this figure in color, go online.

and small curves lies not so much with the shape of $F_L(r)$, but rather the magnitude of $\widehat{\kappa}$, which could arise from differences in ASM mass or activation in airways of different sizes. The ASM tension hysteresis associated with these transfer functions and simulations are given in Fig. 3 *d*. Here the qualitative agreement with the results of Gazzola et al. (9) are striking, with both data sets characterized by monotonic increases in tension with sharp rises at longer lengths, and also a similar characteristic shape (e.g., compare with Fig. 2 in Gazzola et al. (9)).

Comparison between implied tension transfer function and empirical sin^3( ) form

One natural question arising from the implied tension transfer function shape (Fig. 3 *c*) is the relationship with the sin^3( )-type empirical length-tension form. That is, could the implied tension transfer function simply be the ascending branch of the sin^3( ) form? The results in Fig. 2 suggest that there is a significant difference, but making an explicit comparison is instructive. In Fig. 4 *a*, we again show the implied tension transfer functions (for both small and large airways) but with two different versions of the sin^3( ) form overlaid. The first is a naive sin^3( ) form for which the optimal length is taken to be r_0, which is exactly the form used previously. It is immediately apparent that this sin^3( ) form deviates significantly from the implied transfer functions, even considering only the ascending branch. Another possibility is that the ASM optimal length might not be r_0, as suggested by the work of Lee-Gosselin et al. (12) regarding in situ length. If we allow for significant variation between the optimal and in situ length, then the implied tension transfer function does have a strong similarity to the lower portion of the ascending branch of the sin^3( ) form—this is the fit sin^3( ) form in Fig. 4 *a*. That is, for the ascending branch of the sin^3( ) form to be sufficient to explain the data, the ASM in situ would be operating significantly away from the optimal length, on only the lower half of the ascending branch.

Comparison with experimental QSPR inflation data

Another valuable comparison is with the limited QSPR inflation data available. Recall that we have fitted out implied tension transfer functions based on only the

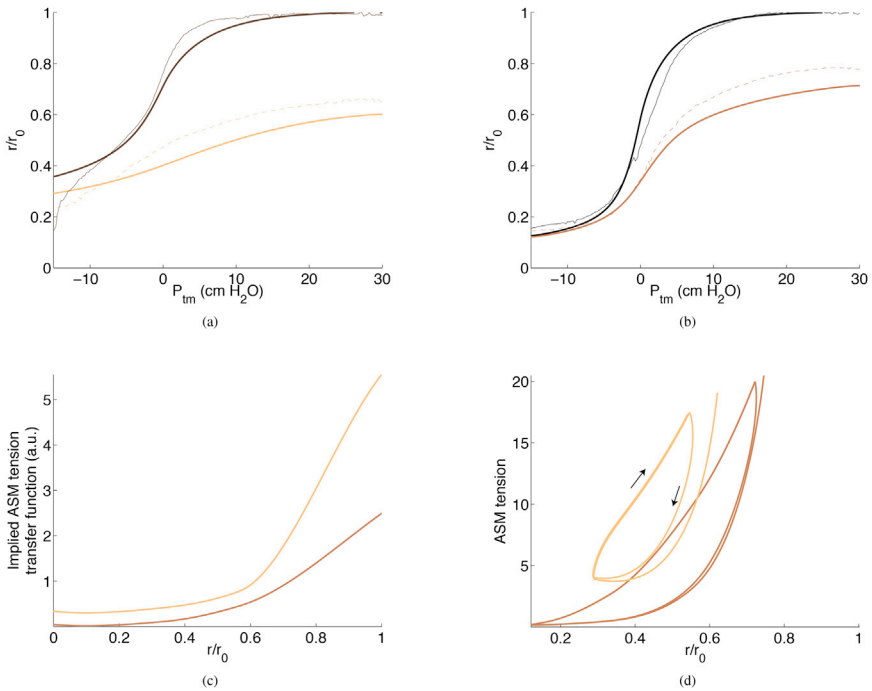

FIGURE 3 Pressure-radius fits and length-tension dependency implied by Harvey et al. (8) data. (*a*) Larger airway deflation pressure-radius curves, relaxed (*darker curve*) and constricted (*lighter curve*). Model simulations are the heavy lines, superimposed over the experimental data of Harvey et al. (8). (*b*) Smaller airway deflation pressure-radius curves, relaxed (*darker curve*) and constricted (*lighter curve*). Model simulations are the heavy lines, superimposed over the experimental data of Harvey et al. (8). (*c*) Implied transfer function required to generate P-R curves in (*a*) and (*b*). The lighter curve is for larger airways, and the darker curve is for smaller airways. Note that the two curves are similar up to a multiplicative scaling factor; see Fig. 4 *a*. (*d*) Length-tension hysteresis curves from the constricted airway simulations in (*a*) and (*b*), using the implied transfer functions given in (*c*). To see this figure in color, go online.

deflation data of Harvey et al. (8). We validate this approach by comparing with the inflation QSPR curves of LaPrad et al. (11) for large bovine airways, but for both baseline and constricted cases. These simulation data are given in Fig. 4 *b* and are both qualitatively and quantitatively similar to those of LaPrad et al. (11) (see Fig. 8 in that article). Specifically there is significant narrowing in both the compliant region, and the relaxed plateau, but little narrowing at low transmural pressures. There is also little increase in hysteresis, with relatively modest hysteresis in both baseline and constricted airways. This suggests the validity of extrapolating the inflation branches using implied tension transfer functions fitted from the deflation data only.

Potential consequences of implied length-tension curves

The implied length-tension curves computed in the previous section could potentially have significant implications for bistable airway behavior in coupled systems. To assess how bistability might change, we extrapolate the inflation branches of each curve, based on the implied tension transfer function fitted to the deflation branch, for different airway sizes and degrees of activation. The results of these simulations are given in Fig. 5, with changes in ASM activation shown in the left panel, and changes in airway order in the right (using the same parameter values and color coding as Fig. 2). Clearly there is a qualitatively different pattern of response to ASM activation, with significant changes in the low-compliance plateau region and little increase in hysteresis as ASM activation is increased (Fig. 5, *left panel*). Similarly there is much less hysteresis in larger airways (Fig. 5, *right panel*). As a result, regions of bistability shrink markedly when compared with the naive modeling assumptions (compare with Fig. 2), with only narrow windows of P_{tm} over which bistability occurs. Increasing ASM activation

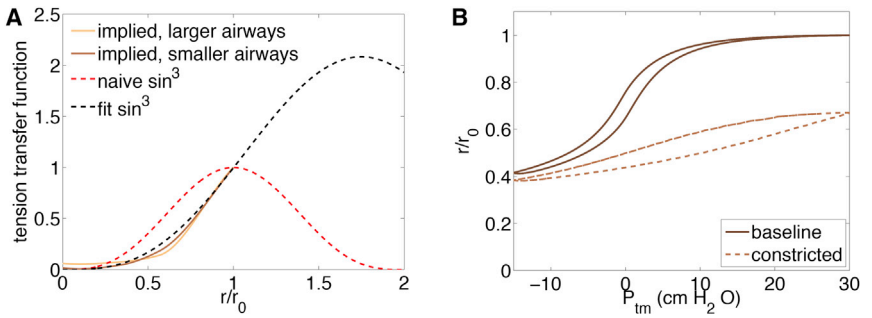

FIGURE 4 Tension transfer function comparison and QSPR inflation curves. (*A*) Comparison of implied tension transfer functions with empirical $\sin^3$ forms, both naive and fitted. The naive $\sin^3$ form assumes that the in situ and optimal ASM lengths are equal, and in this case there is significant discrepancy between the ascending branch and the implied transfer functions. If instead the in situ and optimal ASM lengths are allowed to diverge significantly, then the lower half of the ascending $\sin^3$ branch is a reasonable approximation to the implied transfer function. (*B*) Baseline and constricted QSPR inflation curves for comparison with published inflation data from LaPrad et al. (11) (compare to their Fig. 8). Here the airway is order 22, using the large airway implied tension transfer function, with $\widehat{\kappa} = 0$ and 6 for the baseline and constricted cases, respectively. To see this figure in color, go online.

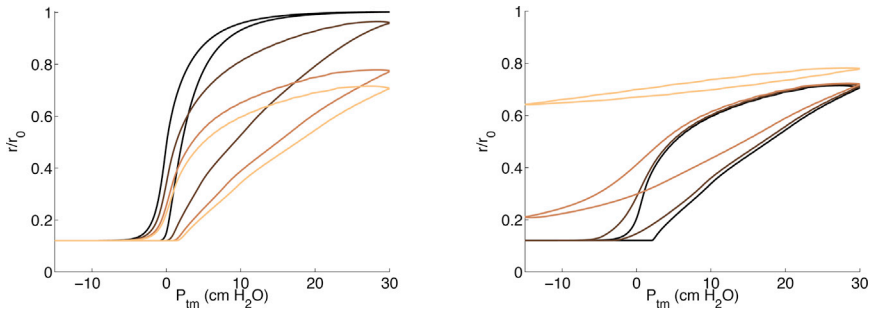

FIGURE 5 Changes in pressure-radius hysteresis curves, using the implied tension transfer function, as ASM activation is varied for fixed order (*left*) and as airway order is varied for fixed activation (*right*). Color coding as in Fig. 2; see annotations in that figure. Note that in the left panel, a relatively small airway (order 5) is used, as in Fig. 2 (*left column*), compared with the relatively large (order 22) airway in Fig. 4 *b*. To see this figure in color, go online.

does not significantly broaden the window of bistability, but instead primarily serves to narrow the open state. Taken together, this indicates a much greater predilection toward airway narrowing rather than airway closure, which if true could have significant implications for coupled airway models. There are several important notes of caution needed for interpreting these results, which are considered more fully in the Conclusions.

CONCLUSIONS

In this article, we have constructed, to our knowledge, a new model of airway constriction with narrowing and transitions between open and closed states modulated by ASM dynamics (represented by a cross-bridge model). In doing so, we show that airway quasi-static pressure-radius hysteresis loops can have qualitatively different characteristics, and that naive modeling yields different qualitative characteristics from recent experimental data. To redress this deficiency, at least partially, we fitted implied length-tension transfer functions needed to capture these missing features, and in doing so we recover the length-tension dependency recently found by Gazzola et al. (9); the consistency of their results with those of Harvey et al. (8), as shown by the model, is an additional step forward in understanding intact airway behavior, though it is important to note that the implied length-tension transfer function we have computed is only a crude representation that gives no direct biophysical basis for the behavior. However, there are several possible interpretations of the implied transmission function. One possible resolution is that the ASM in situ length is significantly shorter than the ASM optimal length, and that the data of both Harvey et al. (8) and Gazzola et al. (9) occur only on the lower part of the ascending branch of a $\sin^3(\ )$-type length-tension relationship (e.g., Fig. 4 *a*). Such a mismatch in lengths is supported by the work of Lee-Gosselin et al. (12). However, there are other possibilities: instead of intrinsic ASM mechanics (e.g., in situ versus optimal length), such behavior could be attributed to (in) effective transmission of ASM force to the airway wall, or to more complex wall behavior such as collagen prestrain or effective mechanical modification of the airway wall in constriction. There is currently insufficient data to pinpoint the precise mechanism; however, the implied transfer function captures the inadequacy of our current models, and suggests several possible resolutions.

We also extrapolated our model results to consider the potential implications of ASM-modulated airway opening/closing transitions to coupled airway models, such as the formation of clustered ventilation defects (e.g., Venegas et al. (6) and Donovan and Kritter (7)). The qualitative features of these curves suggest a greater propensity toward more modest airway narrowing, rather than effective closure, than might have been expected. There are several important caveats in interpreting the Implied ASM Length-Tension Relationship in this context. First, as mentioned previously, the implied L-T transfer function is a crude representation, lacking explicit biophysical basis, which is explicitly fitted only to the deflation branch and extrapolated to the inflation branch. As such, there is an obvious degree of uncertainty about the inflation branches (and hence the extent of the hysteresis and bistability). Similarly, we have not included a passive ASM component (e.g., Donovan et al. (28)), and this might be reasonably expected to contribute disproportionately to the inflation branch. However, perhaps it is more important to emphasize that isolated airway bistability of the sort considered here (akin to Affonce and Lutchen (1)) is not strictly necessary for coupled airway models that drive clustered ventilation defect formation; instead, feedback mechanisms via airflow and parenchymal tethering (2) could introduce bistability in coupled systems, even where isolated airways lack such behavior. That said, decreased bistability in isolated airways would require a greater role for these feedback mechanisms in generating closure (or near closure) leading to clustered ventilation defects in coupled airway systems. Even then, ASM dynamics might continue to play an important role in modulating transitions in these modified coupled system dynamics.

It is important to emphasize that here we have only considered slow, quasi-static behavior (pressure oscillations with an 80 s period; the experiments of Gazzola et al. (9) are slower still at 0.004 Hz). Certainly ASM is known to exhibit different behavior when forced at higher frequencies (29), and airway-ASM coupling on shorter timescales is certainly an area worth investigating more carefully; for example,

Hiorns et al. (4,5) have looked at coupled narrowing dynamics at higher frequencies. However, there is limited data available for higher-frequency behavior of intact segments; even at the low rates considered here, the significant discrepancies between naive models, and the experimental data, suggest that our understanding of airway-ASM interaction is incomplete.

There are also caveats regarding the construction of the airway wall model, where we have opted for a simple construction based around the static equilibria (1) using the model of Lambert et al. (10). Certainly many alternatives are possible. For example, Hiorns et al. (4) constructed a similar model, which couples an ASM cross bridge to an airway wall model, but using a more sophisticated solid mechanics airway wall model. Clearly this significantly increases the computational complexity; although Hiorns et al. (4) do not explicitly consider opening/closing transitions, the qualitative similarity of their results regarding the mutual dependence of ASM dynamics and airway compliance in airway narrowing suggest that many of the same mechanisms are at work. Having decided to use an empirical airway wall model, there are still other choices available. For example, one could use instead the model of Thorpe and Bates (23), which has many similar features; perhaps the best reason for selecting the Lambert model is the recent intact airway data supporting it (8), although replacing the Lambert model with the Thorpe/Bates model, or similar, in this study is unlikely to significantly alter the results.

Coupling the Lambert airway wall model with ASM dynamics could also be done in different ways; here we have applied first-order relaxation dynamics on top of the static equilibria provided by the data. One alternative would be to enforce the static equilibria as algebraic constraints, as done in Politi et al. (20); however, this introduces significant computational challenges (PDEs with algebraic constraints), and furthermore there is no good reason to suppose that the static equations are, in fact, satisfied at all times. It is also possible that the dynamics are entirely more complicated; for example, power law relaxation (e.g., Lenormand et al. (30)), but such a model would add a great deal of complexity and is not currently well supported by data for airway dynamics. On balance, for this study the first-order relaxation kinetics approach offers the best modeling compromise between model complexity and realism, elucidating the underlying coupling mechanisms without undue complications from either analysis or computational cost.

ACKNOWLEDGMENTS

I am grateful to Brian Harvey for providing the experimental data from Harvey et al. (8) used for fitting and shown in Fig. 3, *a* and *b*.

This work was supported by the Marsden Fund from the Royal Society of New Zealand.

REFERENCES

1. Affonce, D. A., and K. R. Lutchen. 2006. New perspectives on the mechanical basis for airway hyperreactivity and airway hypersensitivity in asthma. *J. Appl. Physiol.* 101:1710–1719.
2. Anafi, R. C., and T. A. Wilson. 2001. Airway stability and heterogeneity in the constricted lung. *J. Appl. Physiol.* 91:1185–1192.
3. Anafi, R. C., and T. A. Wilson. 2002. Empirical model for dynamic force-length behavior of airway smooth muscle. *J. Appl. Physiol.* 92:455–460.
4. Hiorns, J. E., O. E. Jensen, and B. S. Brook. 2014. Nonlinear compliance modulates dynamic bronchoconstriction in a multiscale airway model. *Biophys. J.* 107:3030–3042.
5. Hiorns, J. E., O. E. Jensen, and B. S. Brook. 2016. Static and dynamic stress heterogeneity in a multiscale model of the asthmatic airway wall. *J. Appl. Physiol.* 121:233–247.
6. Venegas, J. G., T. Winkler, …, R. S. Harris. 2005. Self-organized patchiness in asthma as a prelude to catastrophic shifts. *Nature.* 434:777–782.
7. Donovan, G. M., and T. Kritter. 2015. Spatial pattern formation in the lung. *J. Math. Biol.* 70:1119–1149.
8. Harvey, B. C., H. Parameswaran, and K. R. Lutchen. 2015. Can breathing-like pressure oscillations reverse or prevent narrowing of small intact airways? *J. Appl. Physiol.* 119:47–54.
9. Gazzola, M., C. Henry, …, Y. Bossé. 2016. Smooth muscle in human bronchi is disposed to resist airway distension. *Respir. Physiol. Neurobiol.* 229:51–58.
10. Lambert, R. K., T. A. Wilson, …, J. R. Rodarte. 1982. A computational model for expiratory flow. *J. Appl. Physiol.* 52:44–56.
11. LaPrad, A. S., T. L. Szabo, …, K. R. Lutchen. 2010. Tidal stretches do not modulate responsiveness of intact airways in vitro. *J. Appl. Physiol.* 109:295–304.
12. Lee-Gosselin, A., C. D. Pascoe, …, Y. Bossé. 2013. Does the length dependency of airway smooth muscle force contribute to airway hyperresponsiveness? *J. Appl. Physiol.* 115:1304–1315.
13. Huxley, A. F. 1957. Muscle structure and theories of contraction. *Prog. Biophys. Biophys. Chem.* 7:255–318.
14. Hai, C.-M., and R. A. Murphy. 1988. Cross-bridge phosphorylation and regulation of latch state in smooth muscle. *Am. J. Physiol.* 254:C99–C106.
15. Mijailovich, S. M., J. P. Butler, and J. J. Fredberg. 2000. Perturbed equilibria of myosin binding in airway smooth muscle: bond-length distributions, mechanics, and ATP metabolism. *Biophys. J.* 79:2667–2681.
16. Stålhand, J., and G. A. Holzapfel. 2016. Length adaptation of smooth muscle contractile filaments in response to sustained activation. *J. Theor. Biol.* 397:13–21.
17. Bates, J. H. 2015. Modeling the impairment of airway smooth muscle force by stretch. *J. Appl. Physiol.* 118:684–691.
18. Ijpma, G., A. M. Al-Jumaily, …, G. C. Sieck. 2011. Myosin filament polymerization and depolymerization in a model of partial length adaptation in airway smooth muscle. *J. Appl. Physiol.* 111:735–742.
19. Wang, L., P. D. Paré, and C. Y. Seow. 2001. Selected contribution: effect of chronic passive length change on airway smooth muscle length-tension relationship. *J. Appl. Physiol.* 90:734–740.
20. Politi, A. Z., G. M. Donovan, …, J. Sneyd. 2010. A multiscale, spatially distributed model of asthmatic airway hyper-responsiveness. *J. Theor. Biol.* 266:614–624.
21. Donovan, G. M. 2013. Modelling airway smooth muscle passive length adaptation via thick filament length distributions. *J. Theor. Biol.* 333:102–108.
22. Keener, J. P., and J. Sneyd. 1998. Mathematical Physiology, Vols. 1 and 2. Springer, New York.

23. Thorpe, C. W., and J. H. Bates. 1997. Effect of stochastic heterogeneity on lung impedance during acute bronchoconstriction: a model analysis. *J. Appl. Physiol.* 82:1616–1625.

24. Dowie, J., T. K. Ansell, …, G. M. Donovan. 2016. Airway compliance and dynamics explain the apparent discrepancy in length adaptation between intact airways and smooth muscle strips. *Respir. Physiol. Neurobiol.* 220:25–32.

25. Brook, B. S., S. E. Peel, …, O. E. Jensen. 2010. A biomechanical model of agonist-initiated contraction in the asthmatic airway. *Respir. Physiol. Neurobiol.* 170:44–58.

26. Lai-Fook, S. J. 1979. A continuum mechanics analysis of pulmonary vascular interdependence in isolated dog lobes. *J. Appl. Physiol.* 46:419–429.

27. Horsfield, K. 1990. Diameters, generations, and orders of branches in the bronchial tree. *J. Appl. Physiol.* 68:457–461.

28. Donovan, G. M., S. R. Bullimore, …, J. Sneyd. 2010. A continuous-binding cross-linker model for passive airway smooth muscle. *Biophys. J.* 99:3164–3171.

29. Fredberg, J. J., D. Inouye, …, S. A. Shore. 1997. Airway smooth muscle, tidal stretches, and dynamically determined contractile states. *Am. J. Respir. Crit. Care Med.* 156:1752–1759.

30. Lenormand, G., E. Millet, …, J. J. Fredberg. 2004. Linearity and time-scale invariance of the creep function in living cells. *J. R. Soc. Interface.* 1:91–97.